Modelling, simulation and control of an electric unicycle

A. Kadis, D. Caldecott, A. Edwards, M. Jerbic
R. Madigan, M Haynes, B. Cazzolato and Z. Prime,
The University of Adelaide, Australia
andrewkadis@gmail.com

Abstract

In this paper the outcomes from a one year honours project to design, build and control a self-balancing electric unicycle, known as the MICYCLE, are presented. The design of the system along with the associated mechanical and electrical components is presented. This is followed by a derivation of the system dynamics using the Lagrangian method which are simulated using Simulink. A linear control strategy to stabilize in the pitch direction is then proposed. Finally, a comparison between the control systems results from the Simulink simulations and experimental results from the physical system is presented.

1 Introduction

The University of Adelaide's School of Mechanical Engineering has a history of encouraging honours students to develop complex systems engineering projects involving the design, build and control of nonlinear, inherently unstable plants. The MICYCLE, shown in Figure 1, is the last in a long series of such projects. These can be seen in Figure 2 and include a double Furuta pendulum [Driver and Thorpe, 2004], self-balancing inline scooters [Clark *et al.*, 2005; Baker *et al.*, 2006], a 6DOF VTOL platform [Arbon *et al.*, 2006], a ballbot [Fong and Uppill, 2009] and an electric diwheel [Dyer *et al.*, 2009].

In March 2010, honours students in the School of Mechanical Engineering at the University of Adelaide commenced the design, build and control of an electric self balancing unicycle called the MICYCLE. The dynamics of single wheeled 'inverted pendulum vehicles, such as the two wheel self-balancing robot [Yamamoto and Chikamasa, 2009], ballbot [Fong and Uppill, 2009] and Segway clones [Clark *et al.*, 2005; Baker *et al.*, 2006] are well known. The manner in which humans regulate pedal powered unicycles has been identified experimentally [Sheng and Yamafuji, 1997]. Numerous electric unicycles have been built that demonstrate self-balancing capability, one of the first being that of Schoonwinkel [1987]. Most early attempts to stabilise the system in the pitch direction used linear controllers: either classical PD controllers [Hofer, 2005, 2006; Blackwell, 2007] or optimal state controllers [Schoonwinkel, 1987; Huang, 2010]. Later control systems employ non-linear strategies for both pitch and roll stabilisation in path tracking [Naveh *et al.*, 1999].

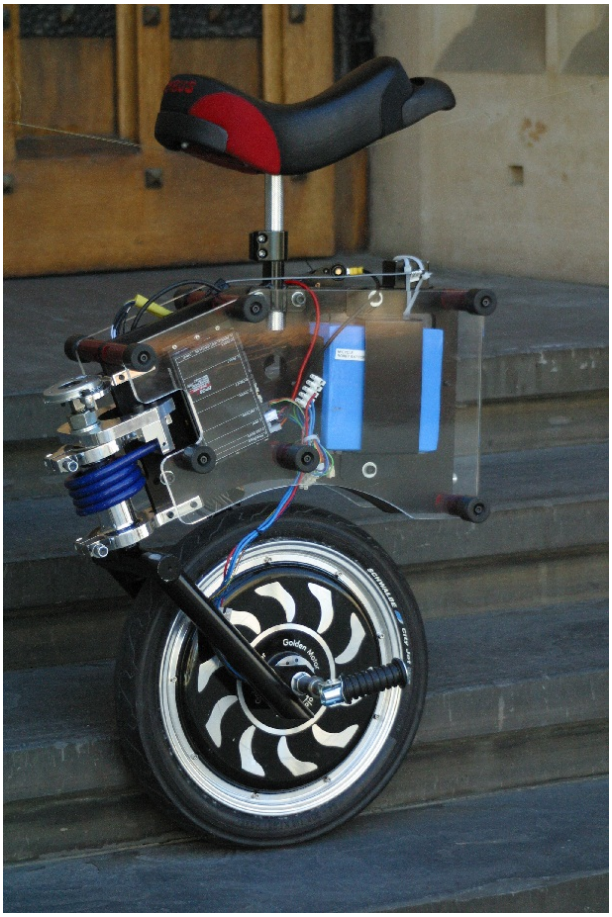

Figure 1: Photograph of the MICYCLE.

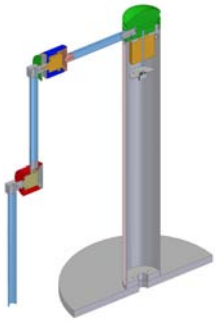

(a) Double Furuta pendulum.

(b) EDGAR scooter.

(c) SON of EDGAR scooter.

(d) 6DOF VTOL.

(e) Ballbot.

(f) Electric Diwheel.

Figure 2: Previous examples of unstable nonlinear underactuated systems built by honours students at The University of Adelaide.

In this paper, the MICYCLE system is discussed in detail. This involves a discussion of the mechanical and electrical components used in the system. The mechanical steering mechanism, used to steer to and to assist the rider in balancing in the roll direction is discussed. Following this, the dynamics of a generic unicycle in the pitch direction are derived using a Lagrangian formulation and simulated in Simulink. A linear PD control law which stabilizes the plant in the pitch direction is then proposed. This controller is implemented on the simulated and physical systems and data from both is used to quantitatively assess the control system.

2 Mechanical and electrical system

The design purview of the MICYCLE was to provide a fully rideable self-balancing electric unicycle which could be learnt to ride in under an hour. To accomplish this, a control system was used to balance the system in the pitch direction and a mechanical steering linkage was designed to assist the rider balancing in the roll direction. The mechanical design, including the steering, and the electrical components, required to implement an embedded control system, are discussed here. These can be seen in a rendered solid model of the MICYCLE, shown in Figure 3.

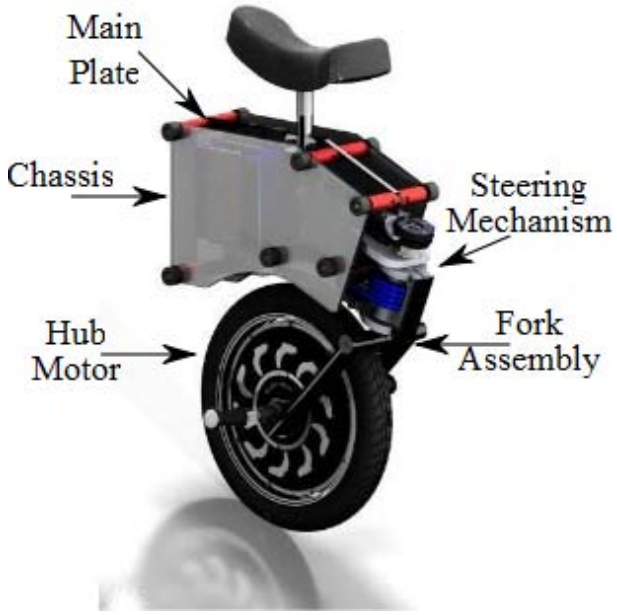

Figure 3: A rendered view showing the of the components of the MICYCLE.

The mechanical elements of the MICYCLE consist of a central plate and a fork assembly to hold the motor. The main plate houses the batteries, microcontroller, power distribution board, inertial measurement unit (IMU) and motor controller. Additionally, the seat and pole on which the rider sits is mounted at the top of the plate. The fork assembly connects the main plate to the hub motor and incorporates a steering mechanism.

The steering mechanism is a major feature of the design. The fork assembly acts as a mechanical linkage between the footpegs and the steering mechanism. The mechanism incorporates a torsion spring to centre the steering arm and a rotary damper to eliminate overshoot and wobble. Additionally, a mechanical limit of $-15°$ prevents oversteering. The end result of this is that when pressure is placed on either of the footpegs, the wheel will turn in that direction independent of the frame. A discussion of the specific geometry of the steering mechanism is beyond

the scope of this paper, but the important dimensions can be seen in Figure 4.

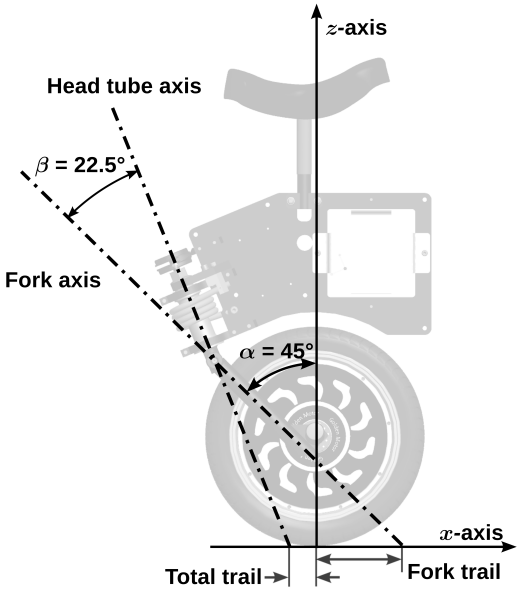

Figure 4: Diagram showing steering geometry design angles.

The steering provides two functions. Firstly, it assists the rider in balancing in the roll direction. When falling to the left, one simply presses on the right footpeg to help stabilise one's self. Although this sounds counter-intuitive, it is very effective in practice. The second function of the steering is that it makes it easy to turn. Typically, a unicyclist must use their arms and hips to twist for turning but the steering mechanism allows smooth turning controlled by simply pressing on the foot pegs.

The system is actuated by a Golden Motors MagicPie MP-16F brushless DC hub motor capable of delivering a maximum torque of 30 Nm at a maximum speed of 250 rpm. The motor is controlled with a maxon motor EPOS2 70/10 motor controller operating in a current control mode, with a current loop bandwidth of 10 kHz. Electrical power is provided by a 36 V, 10 Ah capacity, $LiFePO_4$ battery pack.

The control logic is processed by a Wytec MiniDRAGON-Plus2 Development Board microcontroller, with control state feedback provided by two main sensors. A MicroStrain 3DM-GX2 IMU operating at 300 Hz provides the pitch angle position and pitch angular rate. Hall sensors built into the hub motor return the angular velocity of the wheel, from which the translational velocity of the platform is estimated by a linear velocity approximation. The microcontroller was also used to implement a number of safety features into the system using various safety logic cutoffs. A dSPACE DS1104 prototyping board was also used to design and tune the control system and it is this system and not the embedded one which was used to collect data from the physical system in this paper.

3 Dynamics of the 2DOF system

The dynamics of the Micycle are developed from the inverted pendulum model used extensively in Driver and Thorpe [2004] and further developed in Fong and Uppill [2009]; Huang [2010]; Lauwers *et al.* [2006] to include the translational motion of the pendulum. However, these derivations are inconsistent with regards to coordinate frames and non-conservative forces. Therefore an extensive verification process was undertaken to derive the dynamics of the Micycle. This process was based on the dynamics derived in Nakajima *et al.* [1997]; Nagarajan *et al.* [2009] and through coordinate transforms, verified with the papers discussed above.

The following assumptions have been made in the derivation of the dynamics, with reference to the coordinate system and directions shown in Figure 5.

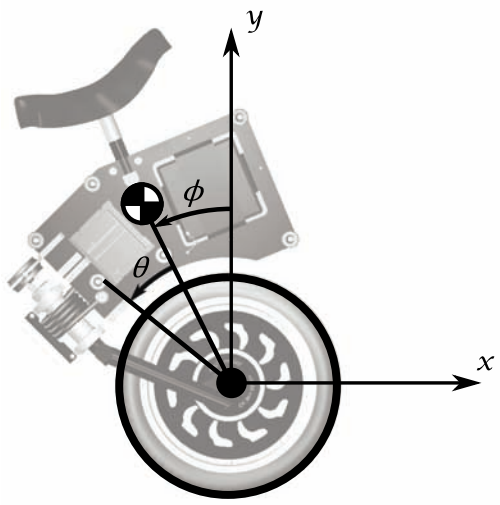

Figure 5: The coordinate system used in the derivation of the system dynamics.

- Motion is restricted to the xy-plane
- A rigid cylinder is used to model the chassis and a vertically orientated thin solid disk used to model the wheel
- Coulomb friction arising from the bearings and tyre-ground contact is neglected, and hence only viscous friction is considered
- The motor is controlled via an intelligent controller in 'current mode' such that the input into the plant is a torque command

Table 1: Constants used to model the MICYCLE.

Symbol	Value	Description
r_w	0.203 m	Radius of the wheel
r_f	0.300 m	Distance to the centre of mass of the frame from the origin
m_w	7.00 kg	Mass of the wheel
m_f	15.0 kg	Mass of the frame
I_f	0.450 kgm^2	Moment of inertia of the frame w.r.t its centre of mass
I_w	0.145 kgm^2	Moment of inertia of the w.r.t its own centre of mass
μ_ϕ	0.08 Nm/(rad/s)	Coefficient of rotational viscous friction (bearing friction and motor losses)
μ_θ	0.05 Nm/(rad/s)	Coefficient of translational viscous friction (rolling resistance)
k_τ	1.64 Nm/A	Motor torque coefficient
g	9.81 m/s^2	Gravitational acceleration

Table 2: Variables used in modelling the MICYCLE.

Symbol	Description
θ	Angular position of the wheel with respect to the frame (anti-clockwise positive)
$\dot{\theta}$	Angular velocity of the wheel
$\ddot{\theta}$	Angular acceleration of the wheel
ϕ	Angular position of the frame with respect to the positive y-axis
$\dot{\phi}$	Angular velocity of the frame (anti-clockwise positive)
$\ddot{\phi}$	Angular acceleration of the frame
τ	Torque applied by the motor, exluding friction
i	Motor supply current

- There is no slip between the tyre and the ground

The model is defined in terms of coordinates ϕ and θ, where:

- ϕ — rotation of the frame about the z-axis
- θ — rotation of the wheel relative to the frame angle

The origin of the right-handed coordinate frame is located at the centre of the wheel, as shown in Figure Figure 5. The positive x-direction is to the right and positive y is upward. The two angular quantities, ϕ and θ, have been chosen such that anti-clockwise rotations about the z-axis are considered positive. The zero datum for the measurement of the frame angle ϕ is coincident with the positive y-axis and the wheel angle θ is measured relative to ϕ.

3.1 Nomenclature

With reference to Figure 5, Tables 1 and 2 define the contants and variables used in the derivation of the plant dynamics that follows in Section 3.2 .

3.2 Non-linear dynamics

The Euler-Lagrange equations describe the dynamic model in terms of energy and are given by:

$$\frac{d}{dt}\left(\frac{\partial \mathcal{L}}{\partial \dot{q}_i}\right) - \frac{\partial \mathcal{L}}{\partial q_i} = F_i$$

where the Lagrangian $\mathcal{L}$ is the difference in kinetic and potential energies of the system, q_i are the generalised coordinates (in this case θ and ϕ) and F_i are the generalised forces. The kinetic and potential energies of the wheel and frame are denoted K_w, V_w, K_f and V_f respectively.

$$K_w = \frac{I_w\dot{\theta}^2}{2} + \frac{m_w(r_w\dot{\theta})^2}{2},$$

$$V_w = 0,$$

$$K_f = \frac{m_f}{2}\left(r_w^2\dot{\theta}^2 + r_f\dot{\phi}\cos\phi\right)^2 + \frac{I_f}{2}\dot{\theta}^2,$$

$$V_f = m_f g r_f \cos\phi.$$

If the generalised coordinates are $\mathbf{q} = \begin{bmatrix} \theta, & \phi \end{bmatrix}^T$, then

$$\frac{d}{dt}\left(\frac{\partial \mathcal{L}}{\partial \dot{\mathbf{q}}}\right) - \frac{\partial \mathcal{L}}{\partial \mathbf{q}} = \begin{bmatrix} 0 \\ \tau \end{bmatrix} - \mathbf{D}(\dot{\mathbf{q}})$$

where

$$\mathbf{D}(\dot{\mathbf{q}}) = \begin{bmatrix} \mu_\theta\dot{\theta}\ , & \mu_\phi\dot{\phi} \end{bmatrix}^T$$

is the vector describing the viscous friction terms. Therefore, the Euler-Lagrange equations of motion can be expressed as

$$\mathbf{M}(\mathbf{q})\ddot{\mathbf{q}} + \mathbf{C}(\mathbf{q},\dot{\mathbf{q}}) + \mathbf{G}(\mathbf{q}) + \mathbf{D}(\dot{\mathbf{q}}) = \begin{bmatrix} 0 \\ \tau \end{bmatrix}.$$

Where the mass matrix, $\mathbf{M}(\mathbf{q})$, is

$$\mathbf{M}(\mathbf{q}) = \begin{bmatrix} I_w + r_w^2(m_f + m_w) & m_f r_w r_f \cos\phi \\ m_f r_w r_f \cos\phi & I_f + r_f^2\cos^2\phi m_f \end{bmatrix},$$

the vector of centrifugal effects, $\mathbf{C}(\dot{\mathbf{q}}, \mathbf{q})$, is

$$\mathbf{C}(\dot{\mathbf{q}}, \mathbf{q}) = \begin{bmatrix} -m_f r_f r_w \dot{\phi}^2 \sin\phi \\ -m_f r_f^2 \dot{\phi}^2 \sin\phi\cos\phi \end{bmatrix},$$

and the vector of gravitational forces, $\mathbf{G}(\mathbf{q})$, is

$$\mathbf{G}(\mathbf{q}) = \begin{bmatrix} 0 \\ -m_f r_f g \sin\phi \end{bmatrix}.$$

These are described in the standard non-linear state space form by defining the state vector, $\mathbf{x} = \begin{bmatrix} \mathbf{q}^T & \dot{\mathbf{q}}^T \end{bmatrix}$, and the input as $u = \tau$. This, together with the above equations gives

$$\dot{\mathbf{x}} = \begin{bmatrix} \dot{\mathbf{q}} \\ \mathbf{M}(\mathbf{q})^{-1}\left(\begin{bmatrix} 0 \\ \tau \end{bmatrix} - \mathbf{C}(\mathbf{q}, \dot{\mathbf{q}}) - \mathbf{G}(\mathbf{q}) - \mathbf{D}(\dot{\mathbf{q}})\right) \end{bmatrix} = f(\mathbf{x}, u)$$

4 Electromechanical system dynamics

The derivation of the mechanical dynamics assumes a motor torque input into the system. In practice, the torque is controlled by the motor controller operating in current mode. There exists a linear relationship between the motor supply current and the resultant motor torque:

$$t = k_t i$$

where τ is the motor torque, $k_t = 1.64\,\mathrm{Nm/A}$ is the motor torque constant and i is the motor supply current. The torque constant was deduced experimentally.

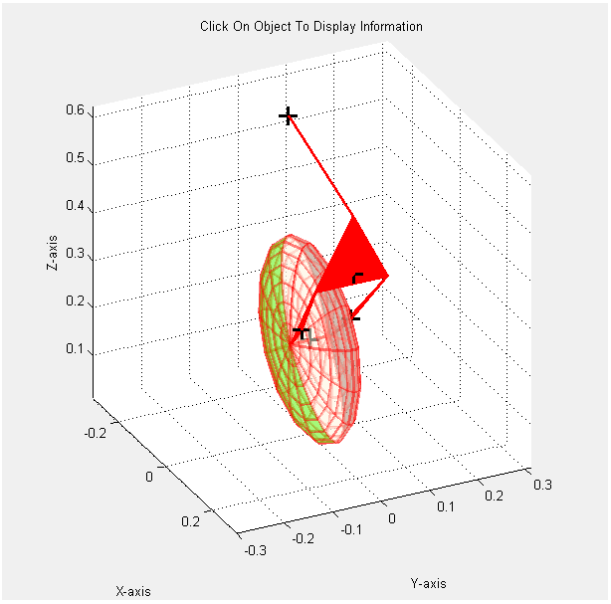

Figure 6: Wireframe view of the SimMechanics model showing linkages and centres of mass.

Table 3: Variables used in modelling the MICYCLE.

Parameter	Value	Description
K_p	800 A/rad	Proportional gain
T_d	0.1 sec	Derivative time constant
$\frac{T_d}{N}$	0.01 sec	Low pass filter time constant

5 State Estimation

There are two states which the control system is required to measure. These are ϕ and $\dot{\phi}$, the angular position and angular rate of the frame respectively. Figure 7 shows how these states are read from the IMU. Note that the $\dot{\phi}$ value is read directly from the IMU rather than differentiating the ϕ value. This is because there is less latency in the $\dot{\phi}$ filters than the ϕ filters. However, the filter implemented with the IMU are proprietary. It is known that the $\dot{\phi}$ filters are slower than the ϕ filters, but no other specifics are known about their structure or frequency response. Thus, the $\dot{\phi}$ was read directly from the IMU rather than differentiating ϕ.

6 PD controller

The control strategy employed here uses a standard proportional-derivative (PD) controller. The implementation of this controller can be seen in Figure 7. The reason for why a PID controller was not used is that a human naturally acts to reduce the steady state error and the addition of integral control can degrade the performance of the controlled response [Clark *et al.*, 2005].

A low pass filter was used on the derivative control term to make the controller proper and to filter out noise from the sensors in the physical system. The parameters of the tuned control system are presented in Table 3. The transfer function for the designed PD controller is presented in Equation (1). Note that strictly speaking, the system actually consists of two distinct transfer functions, one for ϕ and one for $\dot{\phi}$, as different sensors are used for each state. Nevertheless, this is a PD controller and Equation (1) represents the effective transfer function with the two feedback terms combined.

$$G_c = K_p\left(1 + \frac{sT_d}{1 + s\frac{T_d}{N}}\right) \tag{1}$$

7 Numerical simulations

The differential equations derived in Section 3 were modelled within Simulink. For validatation of this simulation, a parallel model was constructed using SimMechanics as shown in Figure 6. Additionally, a virtual reality

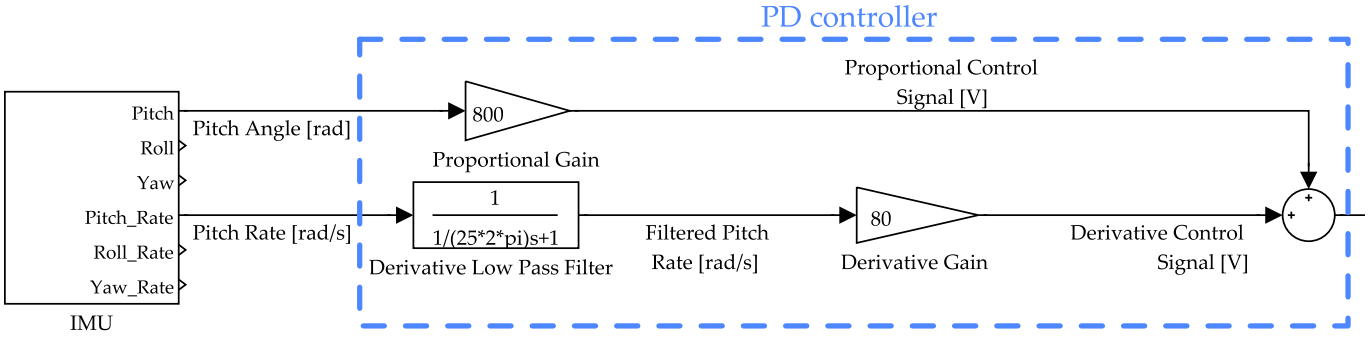

Figure 7: Simulink block diagram representing the state estimation and the PD controller.

(VR) model developed from the Simulink implementation was also built to aid in the visualisation of the plant performance.

The control strategy detailed in Section 6 was then integrated into the Simulink model. This was used to generate numerical simulations of the closed loop system response, presented in Section 8.

8 Experimental data

Data was collected on the physical MICYCLE system and compared to the results obtained from the corresponding numerical simulations.

8.1 Testing methodolgy

Despite the fact that the MICYCLE is fully functional as an embedded system, it is not possible to collect data when it is being run off a microcontroller. Thus it was necessary to run the control system in Simulink through a dSPACE DS1104 prototyping board for data acquisition. As the MICYCLE does not balance in the roll direction without a rider, it was necessary to constrain the wheel so that it would not move. This experimental setup is shown in Figure 8.

The experimental procedure involved offsetting the frame from the vertical axis by a known angle and releasing it. The initial position of the frame, ϕ, acts as a disturbance to the plant and the performance of the control system is assessed through the ability to return the system to 0°.

To allow the numerical simulations to correlate with the physical data, the Simulink model of the system dynamics was modified to reflect this constraint. The wheel angle, θ, was set to a fixed value of 0° and ϕ was set to the appropriate initial position.

It should be noted that although this does not quite represent real world operation of the MICYCLE, this methodology offered a means of being able to quantiatively assess the performance of the physical control system compared to the simulated system. In riding the MICYCLE it has been found that the control system does indeed possess a limited ability to reject disturbances such as bumps and slopes. Nevertheless, these are difficult to quantify and thus the chosen method was adopted.

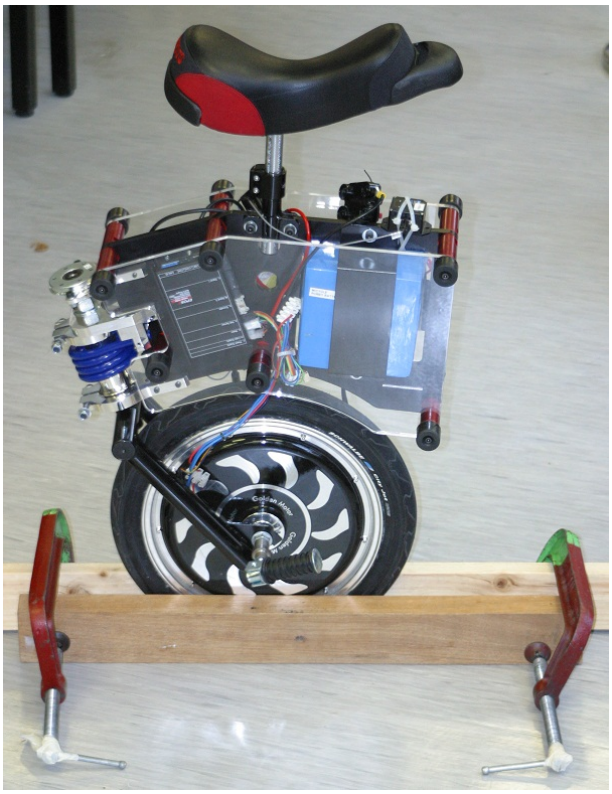

Figure 8: Photograph of the MICYCLE with the wheel constrained as used in testing. Note the clamps at either end of the timber fix the translational position of the system while allowing the frame to rotate about the wheel.

8.2 Experimental closed loop PD controller

The above methodology was then applied to the physical and simulated MICYCLE systems. The results can be seen in Figures 9, 11, 10 and 12.

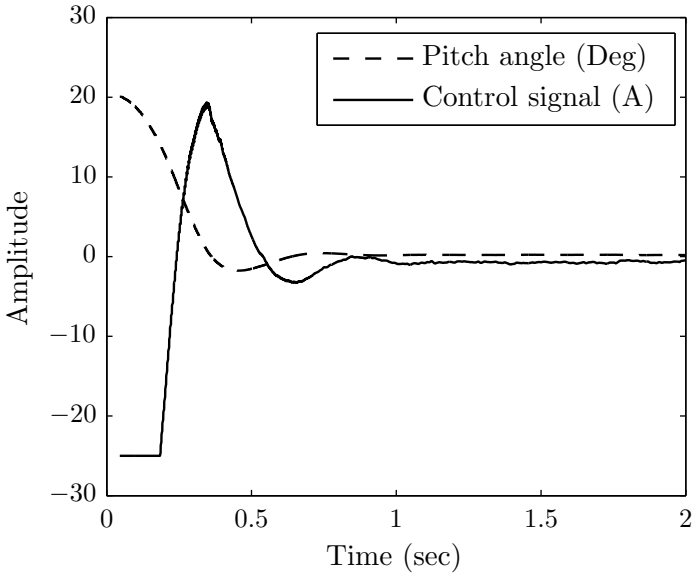

Figure 9: Closed loop response of the constrained physical MICYCLE system when rotated to 20° and released.

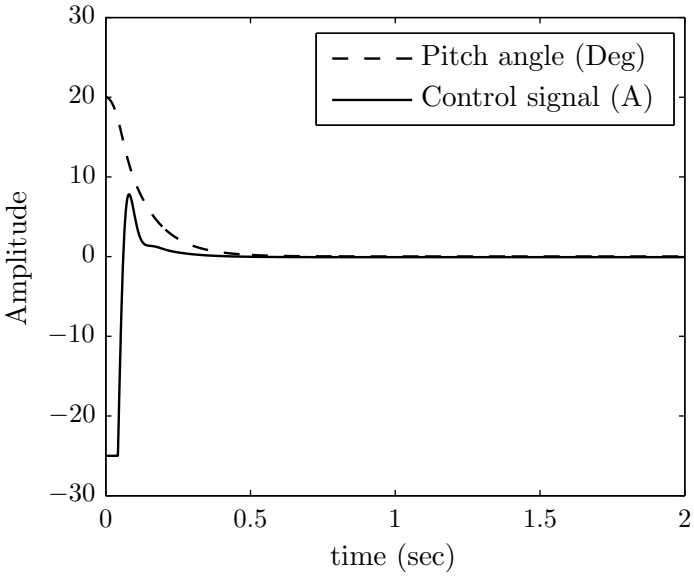

Figure 11: Closed loop response of the constrained simulated MICYCLE system when rotated to 20° and released.

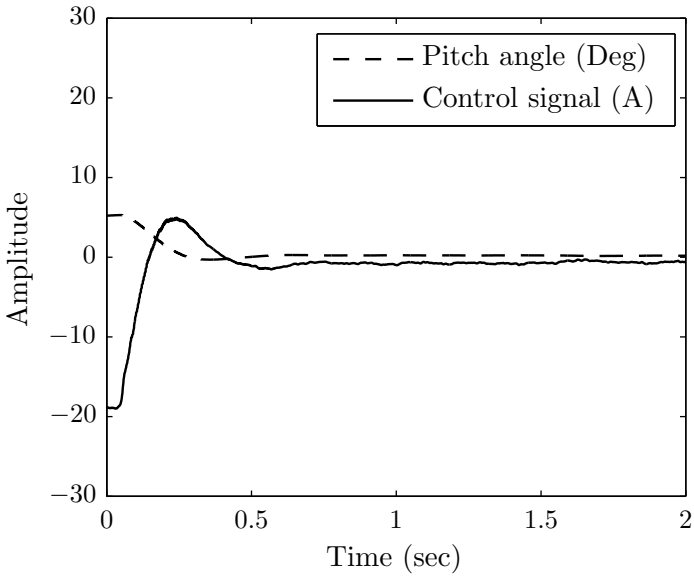

Figure 10: Closed loop response of the constrained physical MICYCLE system when rotated to 5° and released.

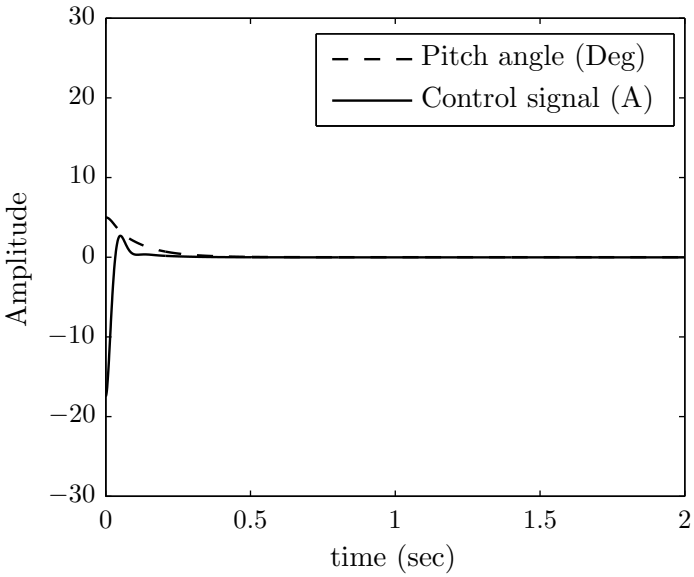

Figure 12: Closed loop response of the constrained simulated MICYCLE system when rotated to 5° and released.

These results demostrate three main points. The first is that the control system suffices for both the simulated and physical systems. The second is that the response of the simulated system is superior to that of the physical system. Finally, the controller has a strong tendency to saturate.

Both the physical and simulated systems present a control system which is able to maintain control authority of an inherently unstable plant in response to a disturbance. Rise times are less than a quarter of a second and there is minimal overshoot, rendering this a suitable control system to be used in a self-balancing unicycle to be ridden by a human. This corellates with what has been experienced in riding the MICYCLE, where it is fully rideable and has the ability to resist small disturbances.

The response of the simulated system is superior to that of the physical system in that it exhibits less overhsoot and a faster response. It is thought that the physical system has a time delay in the control system which is currently unmodelled in the simulated system. This would add phase lag in the control system leading to more overshoot in the response. The simulated system was rerun with time delays modelled in the ϕ and $\dot{\phi}$ feedback terms and it was possible to generate a similar response to the physical system. However, it is suspected that the discrepancy is not merely the result of a pure time delay, but also effected by the frequency response of the filters used on the IMU sensor values. Unfortunately, these filters are proprietary and the specific details of their implementation is not known.

Finally, it is worth highlighting the fact that the motor saturates in all cases. However, this does not appear to be particulary detrimental to the control of the system. The saturated torque is still sufficient to overcome gravity and lift the frame. It is important to realise that in riding the MICYCLE, a more typical use case, there will not be such a propensity for the motor to saturate. This is because a rider will not typically see angular disturbances as large as 20°. Smaller angular disturbances with a larger m_f, due to the additional mass of the rider, are more common and these will be less likely to saturate. The high degree of saturation observed in the presented results is a consequence of the large proportional error induced in this specific testing methodology. That said, it is recognised that there is a strong tendency for the actuator to saturate and a higher degree of control authority is desirable. This is mainly due to the difficulty in procuring a higher capacity brushless DC motor controller and is something that needs to be further investigated.

9 Conclusion and future work

In this paper the dynamics of the unicycle were derived and presented. Numerical simulations were used to verify this derivation. This information was then used to simulate a PD controller whose performance was then compared with that of the physical MICYCLE system.

Future work includes the development of a model based non-linear controller and a backstepping controller. These control strategies will be compared and benchmarked, with the optimal strategy being implemented into the MICYCLE design. A higher capacity motor controller shall also be integrated into the system to alleviate the high tendency to saturate. Another planned development is the addition of active stabilisation in the roll direction. This will use either a reaction wheel or a control moment gyroscope and this actuator will allow the MICYCLE to be a completely self-balancing electric unicycle.

Acknowledgements

The authors would like to acknowledge the support of the Steve Kloeden, Phil Schmidt, Dr. Michael Riese, Norio Itsumi and Silvio De Ieso for their efforts in constructing the physical MICYCLE used in this paper.

References

R. Arbon, E. Arcondoulis, M. Gilmour, and R. Matthews. The WASP: Wired Aerofoil Stabilised Platform. Honours thesis, The University of Adelaide, 2006.

N.P. Baker, C.P. Brown, D.R.S. Dowling, J.L. Modra, and D.J. Tootell. SON of EDGAR: State-space cONtrol of Electro-Drive Gravity-Aware Ride. Honours thesis, The University of Adelaide, 2006.

T. Blackwell. The electric unicycle, 2007.

M.A. Clark, J.B. Field, S.G. McMahon, and P.S. Philps. EDGAR: A self balancing scooter. Honours thesis, The University of Adelaide, 2005.

J. Driver and D. Thorpe. Design, build and control of a single/double rotational inverted pendulum. Honours thesis, The University of Adelaide, 2004.

C. Dyer, K. Fulton, J. Harvey, E. Schumann, and T. Zhu. E.D.W.A.R.D. - Electric Diwheel With Active Rotation Damping. Honours thesis, The University of Adelaide, 2009.

J. Fong and S. Uppill. Design and build a ballbot. Honours thesis, The University of Adelaide, 2009.

K. Hofer. Electric vehicle on one wheel. In *IEEE Vehicle Power and Propulsion Conference*, pages 517–521, 2005.

K. Hofer. Observer-based drive-control for self-balanced vehicles. In *Proceedings of IEEE /IECON 32nd. Annual Conference on Industrial Electronics*, pages 3951 – 3956, 2006.

C.N. Huang. The development of self-balancing controller for one-wheeled vehicles. *Engineering*, 2:212–219, 2010.

T.B. Lauwers, G.A. Kantor, and R.L. Hollis. A dynamically stable single-wheeled mobile robot with inverse mouse-ball drive. In *in Proc. IEEE Int'l. Conf. on Robotics and Automation*, pages 2884–2889, 2006.

Umashankar Nagarajan, Anish Mampetta, George A. Kantor, and Ralph L. Hollis. State transition, balancing, station keeping, and yaw control for a dynamically stable single spherical wheel mobile robot. In *Robotics and Automation, 2009. ICRA '09. IEEE International Conference on*, pages 998 –1003, May 2009.

R. Nakajima, T. Tsubouchi, S. Yuta, and E. Koyanagi. A development of a new mechanism of an autonomous unicycle. In *Proceedings of the 1997 IEEE/RSJ International Conference on Intelligent Robots and Systems. IROS '97.*, volume 2, pages 906 – 912, 1997.

Y. Naveh, P.Z. Bar-Yoseph, and Y. Halevi. Nonlinear modeling and control of a unicycle. *Dynamics and Control*, 9(4):279–296, 1999.

A. Schoonwinkel. *Design and test of a computer stabilized unicycle*. PhD thesis, Stanford University, 1987.

Z. Sheng and K. Yamafuji. Postural stability of a human riding a unicycle and its emulation by a robot. *IEEE Transactions on Robotics and Automation*, 13(5):709 – 720, 1997.

Y. Yamamoto and T. Chikamasa. Nxtway-gs (self-balancing two-wheeled robot) controller design, 2009.